



Eddy-induced cross-slope exchange maintaining summer high productivity of the Bering Sea shelf break

Kohei Mizobata,¹ Jia Wang,¹ and Sei-ichi Saitoh²

Received 30 September 2005; revised 13 June 2006; accepted 14 July 2006; published 31 October 2006.

[1] Eddy-related cross-slope exchange along the Bering Sea shelf break was investigated using a hydrographic observations data set and a numerical model. Results of observations in summer of 2001 showed a shelf break front that formed at a shelf break near an anticyclonic eddy, high nitrate-nitrite concentrations in the subsurface layer, and high chlorophyll *a* (*Chl-a*) concentrations ($\geq 6 \text{ mg m}^{-3}$) in the surface layer. A hydrographic observation in summer of 2002 exhibited relatively high *Chl-a* concentrations at the surface around the anticyclonic eddy. Tracer experiments revealed two types of cross-slope exchange. Under isopycnals, nutrient-rich water in the basin is transported to the shelf and there is about a 64.53% increase in integrated nitrate-nitrite on-shelf flux (50 m depth \sim bottom), when mesoscale eddies are formed and propagated along the shelf break. At the surface, high *Chl-a* waters in the shelf are advected to the deep basin area by eddy transport and propagation. These indicate that (1) mesoscale eddies supply nutrients and sustain primary productivity at the shelf break, and (2) eddies expand the high *Chl-a* area to the basin, then to the highly productive area, so that the Green Belt is maintained.

Citation: Mizobata, K., J. Wang, and S.-I. Saitoh (2006), Eddy-induced cross-slope exchange maintaining summer high productivity of the Bering Sea shelf break, *J. Geophys. Res.*, *111*, C10017, doi:10.1029/2005JC003335.

1. Introduction

[2] The Bering Sea Green Belt named by *Springer et al.* [1996] is an area of high productivity around the Bering Sea shelf break (Figure 1). Biological characteristics of this area include the extreme magnitude and timing of high primary production. Primary production of the Green Belt starts to rise during spring and is up to $175 \sim 275 \text{ g C m}^{-2} \text{ year}^{-1}$ by July, while the spring and autumn phytoplankton blooms occur in the deep ocean, including the Bering Sea shelf region. There should be dynamic mechanisms supporting summer high productivity of the Green Belt, such as nutrient fluxes.

[3] Along the Bering Sea shelf break, tidal mixing, the Bering Slope Current (BSC) and mesoscale eddies have been thought to be the factors generating nutrient fluxes [e.g., *Springer et al.*, 1996; *Stabeno et al.*, 1999; *Mizobata et al.*, 2002]. Recently *Mizobata and Saitoh* [2004] showed the maximum primary production and high eddy variability along the Bering Sea shelf break during summer, and a positive correlation between primary production and the variability of eddy fields using satellite remote-sensing data analysis. This allows us to infer that mesoscale eddies contribute to the primary productivity of the Bering Sea Green Belt. At the present time, vertical-nutrient supply and

cross-slope exchange are recognized as the eddy-related phenomena which supply nutrients.

[4] Vertical transport of nutrients by mesoscale eddies has been detected by previous hydrographic observations [*Sapozhnikov*, 1993; *Mizobata et al.*, 2002]. In the western Bering Sea, *Sapozhnikov* [1993] observed a renewal of waters in the oxygen minimum layer and upwelling of deep waters caused by strong anticyclonic eddies. He also indicates that the intensity of eddy formation contributes to annual primary production and the quantity of nutrients. At the eastern Bering Sea shelf break, *Mizobata et al.* [2002] observed a cyclonic eddy and an anticyclonic eddy. Their hydrographic observations revealed that isopycnals were uplifted, indicating upwelling with nutrient-rich water inside eddies. They suggested that relatively high chlorophyll *a* (*Chl-a*) distributions follow the vertical nutrients supply around the periphery of an anticyclonic eddy or the center of a cyclonic eddy.

[5] Cross-slope exchange has also been observed by satellite-tracked drifters that were deployed around eddies [*Stabeno and van Meurs*, 1999; *Mizobata and Saitoh*, 2003]. *Stabeno and van Meurs* [1999] deployed 13 drifters in the southeastern Bering Sea. Seven drifters moved northward along the shelf, while trajectories of the other six drifters revealed meanders or eddies and on-shelf flow. Also, they estimated an on-shelf transport of $0.75 \times 10^6 \text{ m}^3 \text{ s}^{-1}$, almost the same as the transport through the Bering Strait ($0.8 \times 10^6 \text{ m}^3 \text{ s}^{-1}$), indicating that the on-shelf flux is not negligible. Our drifter trajectories in 2001 and 2002 are shown in Figure 2. Satellite-tracked drifters were deployed on July 26, 2001 [*Mizobata and Saitoh*, 2003], and August 10, 2002, by T/S *Oshoro-Maru*, Faculty of Fisheries, Hokkaido University. The drifter in 2001 (solid line)

¹International Arctic Research Center, University of Alaska Fairbanks, Fairbanks, Alaska, USA.

²Laboratory of Marine Bioresource and Environment Sensing, Graduate School of Fisheries Sciences, Hokkaido University, Hokkaido, Japan.

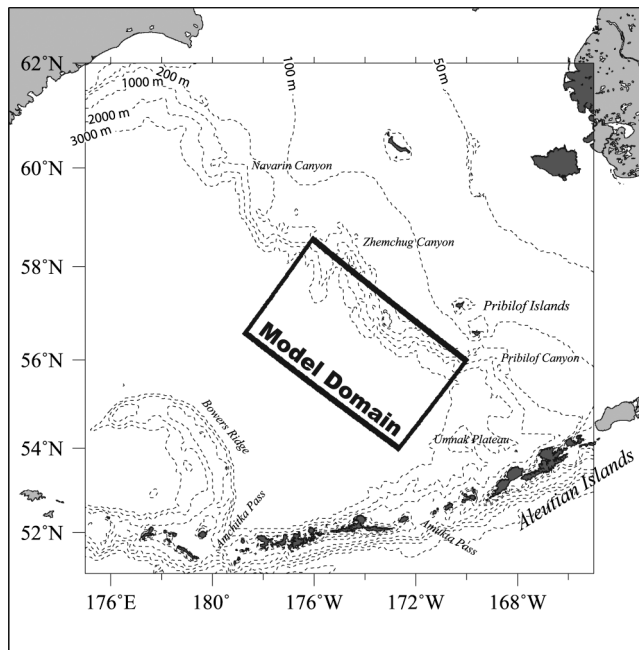


Figure 1. The Bering Sea shelf break represented by 50, 100, 200, 1000, 2000, 3000 m isobaths and the model domain are shown. The model domain includes complex shelf break features including Zhemchug Canyon.

captured the anticyclonic eddy during July 26 to August 1 and then moved onto the shelf, while the drifter in 2002 (dashed line) moved along 1000-m isobaths and then to the basin on August 24 after tracking the anticyclonic eddy. This cross-slope exchange in relation to eddy is thought to transport nutrients and biota from the basin to the shelf [Stabeno and van Meurs, 1999; Okkonen, 2001]. In the Gulf of Alaska, Ladd *et al.* [2005] concluded that the high concentration of nitrate in the deep basin must be transported to the shelf due to cross-slope exchange induced by downwelling relaxation, eddies, and the combination of strong bathymetric gradients and tidal mixing. On the other hand, cross-slope exchange similar to our drifter study result is sometimes observed, and is thought to be an episodic event [Stabeno and van Meurs, 1999].

[6] Although several studies of the Bering Sea eddy field and primary productivity at the shelf break have been undertaken, we still have questions to be resolved. For instance, vertical nutrient supply alone cannot explain summer high productivity because the region from the shelf break to the basin is a high-nutrient, low-chlorophyll (HNLC) region. In addition, the depth of a drifter's drogue is 15 m to about 50 m, which can capture only surface flow, so that the structure and timing of cross-slope exchange is poorly understood below the 50 m depth, where nutrient-rich water can be found. Also Bering Sea eddies at the shelf break should exhibit basin-ward transport as do eddies in the California Current, Gulf Stream and Alaska Gyre [Miller *et al.*, 1999; Lin and Atkinson, 2000; Mackas and Galbraith, 2002; Okkonen *et al.*, 2004; Ladd *et al.*, 2005; Whitney *et al.*, 2005; Peterson *et al.*, 2005]. Okkonen *et al.* [2004] showed high chl-*a* concentrations induced by an anticyclonic eddy at the Bering Sea shelf break during spring. In the Gulf of Alaska, offshore transports of

nutrients and coastal biota by an anticyclonic eddy are evident [Ladd *et al.*, 2005; Whitney *et al.*, 2005; Peterson *et al.*, 2005], but the effects of this basin-ward transport on primary production during summer have not yet been investigated in this region. The three-dimensional cross-slope exchange by eddies has, therefore, yet to be resolved, and the details of Bering Sea eddy effects on new/primary production at the shelf break remain to be elucidated.

[7] To address these questions, we will (1) clarify the three dimensional cross-slope exchange due to eddies and (2) explore the mechanism maintaining summer high productivity of the Bering Sea Green Belt using an integration/synthesis approach that combines hydrographic observation and satellite data, and a three-dimensional ocean general circulation model.

[8] This paper is organized as follows. Section 2 describes the details of hydrographic stations for detecting mesoscale eddies and a numerical model for the simulation of cross-slope exchange. The water properties, nutrient (nitrate + nitrite) distribution and *Chl-a* distribution around anticyclonic eddies in the Bering Sea are shown in section 3. Eddy-related on-shelf flux and basin-ward transport simulated by a numerical model are presented in section 4. In section 5, we discuss the results and summarize this study.

2. Data and Methods

2.1. Field Measurements

[9] The observations of Bering Sea anticyclonic eddies by T/S *Oshoro-maru* (Faculty of Fisheries, Hokkaido University) were conducted at the shelf break around the Pribilof Islands from July 25 to 26, 2001, and from August 8 to 9, 2002 (Figure 3). The 11 and 8 hydrographic stations in 2001 and 2002 were interpolated at intervals of about 10 nautical miles to survey the structure of a mesoscale eddy.

[10] To detect the location of mesoscale eddies and determine hydrographic stations before the observations, we utilized TOPEX (TOPOgraphy EXperiment for Ocean Circulation)/ERS (European Remote Sensing Satellite)-2 daily sea level anomaly (SLA) images from the CCAR (Colorado Center for Astrodynamics Research) Altimeter Data Sets (<http://www-ccar.colorado.edu/research/topex/html/topex.html>). Figure 3 shows hydrographic stations and SLA maps derived from 1/3° gridded TOPEX/Poseidon, Jason-1 and ERS-1/2 SLA data sets provided by Archiving Validation and Interpretation of Satellite Data in Oceanography (AVISO). Note that SLA maps in Figure 3 show anomalies after the mean circulation field (i.e., an open meander of the geostrophic current looks like a closed eddy) has been eliminated. Altimeter maps show that along the shelf break the anticyclonic eddy, rather than the cyclonic eddy, tends to occur (Figure 3). Oceanic mesoscale eddies frequently emerge along a strong current, such as the boundary current (e.g., Kuroshio). In addition, the diameter of the anticyclonic eddies averaged about 100 km (about 1° in latitudinal direction). Since the size of a mesoscale eddy depends on the wavelength of the strong current. Figure 3 implies that these mesoscale eddies are related to the existence of the typical BSC which has a wavelength of about 200 km along the shelf break [Okkonen, 2001].

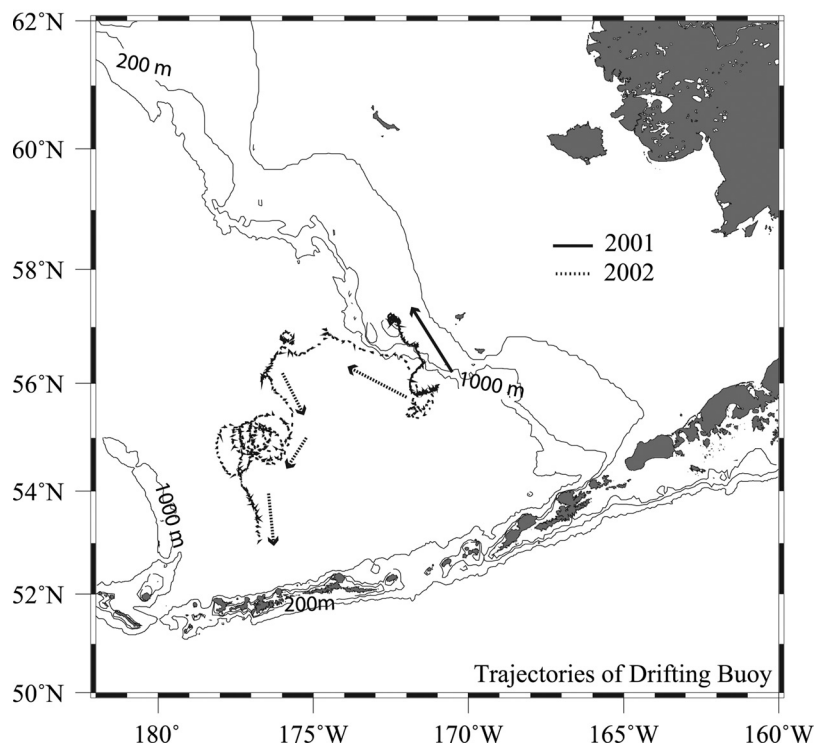


Figure 2. Trajectories of a drifting buoy in 2001 and 2002 at the eastern shelf break are shown. Black lines and dotted lines indicate each trajectory in 2001 and 2002, respectively.

[11] We then focused on the anticyclonic eddy near the shelf break. In the summer of 2001 and 2002, relatively weak or small anticyclonic eddies near the Pribilof Islands were observed, while strong anticyclonic eddies were located near the Zhemchug Canyon. At every station, the conductivity/temperature/depth (CTD, SeaBird SBE-9 plus)-Rosette cast was carried out with 12 niskin bottles from the surface to the bottom or 1500 m depth, whichever was less. Vertical profiles of temperature and salinity were averaged over 1 m intervals. Conductivity was measured using a salinometer calibrated with standard seawater.

[12] It is important to examine the nutrient and *Chl-a* dynamics along the shelf break near the Pribilof Islands because these are highly productive fishing grounds [BEST, 2003]. Seawater samples were collected by 12 niskin bottles on the CTD-Rosette system from the surface to a depth of 200 m. *Chl-a* concentrations were measured using a Turner Designs 10-AU Field Fluorometer after extracting *Chl-a* using N,N-dimethylformamide (DMF). Nutrient concentrations (nitrate-nitrite, phosphorus, and silicate) were determined by the Laboratory of Marine Environmental Science, Graduate School of Fisheries Sciences, Hokkaido University, using a Technicon Autoanalyzer II, which can measure nutrient concentrations by a colorimetric analysis applying Beer-Lambert's law. In this paper we will present nitrate-nitrite concentration, because water samples for phosphorus concentrations in 2002 were contaminated and not measured.

2.2. Numerical Simulation of the Eddy Field and the Cross-Slope Exchange

[13] The Estuarine, Coastal and Ocean Model with a semi-implicit scheme (hereafter referred to as ECOM-si [Blumberg, 1991; Wang and Ikeda, 1997a]) was applied

to simulate the eddy field and the cross-slope exchange at the Bering Sea shelf break. The ECOM-si is described in detail by Blumberg [1991] and Wang and Ikeda [1997a]. In this paper, we introduce the main features of ECOM-si. The ECOM-si is almost the same as the Princeton Ocean Model (POM [Blumberg and Mellor, 1987]) with horizontal curvilinear coordinates, Arakawa-C Grid [Arakawa and Lamb, 1977], sigma vertical coordinates, a free surface, and a second-order turbulence closure model for vertical viscosity [Mellor and Yamada, 1982]. The differences are (1) a semi-implicit scheme for calculating the surface elevation in the shallow water equations [Casulli, 1990], (2) no use of the mode-splitting method, and (3) use of a predictor-corrector scheme [Wang and Ikeda, 1995, 1997a] to remove the inertial instability due to use of the Euler forward scheme in time in the original ECOM-si [Blumberg, 1991]. ECOM-si with a predictor-corrector scheme is suitable for simulating unstable baroclinic waves and mesoscale eddies in a very low viscosity environment.

[14] The model domain is 100×60 horizontal grid points extending from the shelf break near the Pribilof Islands to the basin with southeast and northwest open boundaries (Figure 1). The eddy-resolving resolution of this model is $5 \text{ km} \times 5 \text{ km}$, which is less than half the internal baroclinic Rossby radius of deformation (R_d) is estimated to be about 10.67 km at 58°N because we need to simulate mesoscale eddies. Twenty-one sigma vertical levels (0.0, -0.04 , -0.08 , -0.115 , -0.15 , -0.185 , -0.22 , -0.255 , -0.29 , -0.33 , -0.4 , -0.47 , -0.54 , -0.61 , -0.68 , -0.75 , -0.8 , -0.85 , -0.9 , -0.95 , -1.0) were used. Bathymetry was derived from a 5-minute ETOPO5 global elevation model.

[15] The initial temperature, salinity and northwestward geostrophic velocity calculated using the temperature and

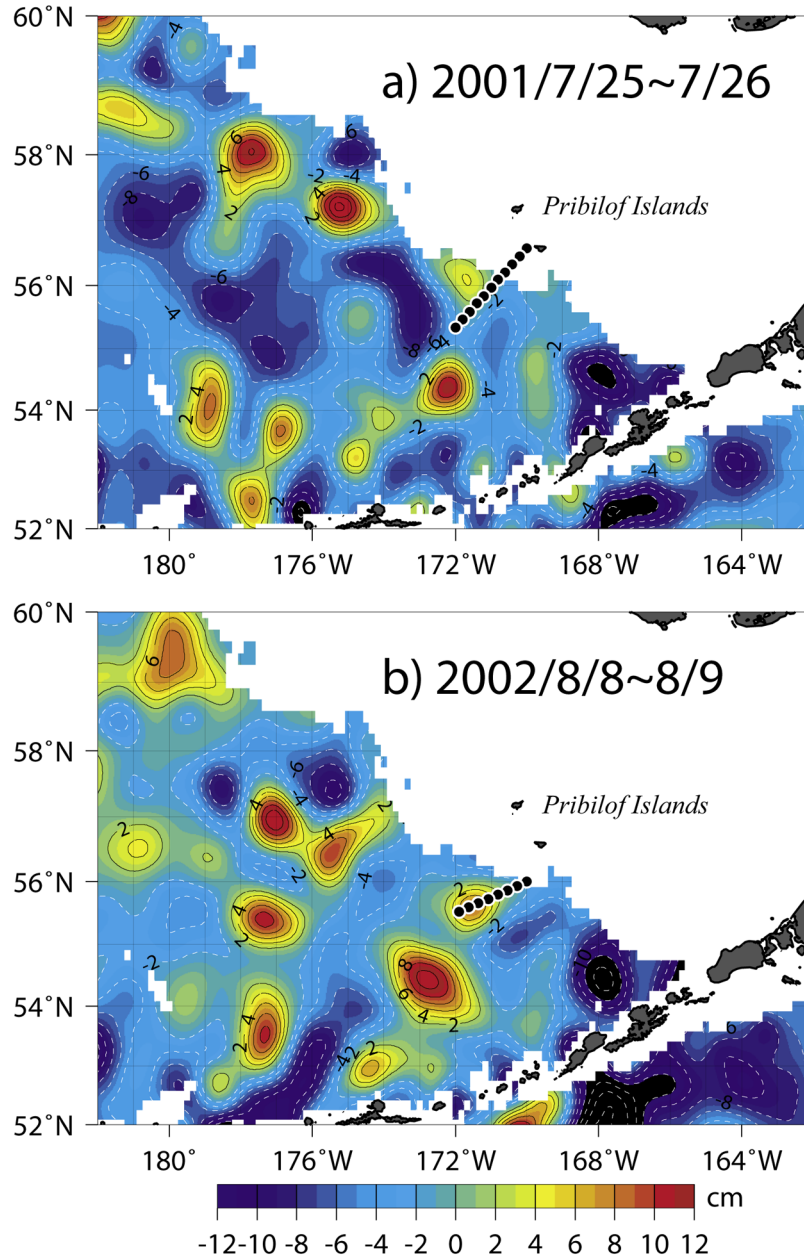


Figure 3. Hydrographic stations (a) July 25 to 26, 2001, and (b) from August 8 to 9, 2002, are shown. Note that sea level anomaly (SLA) map is on July 25 and August 7 derived from AVISO (Archiving Validation and Interpretation of Satellite Data in Oceanography) $1/3^\circ$ SLA data sets.

salinity are shown in Figure 4. To achieve jet flow like that of the BSC, the cross-slope isopycnal tilt was given in this model. Because our numerical experiments did not use the spin-up integration, the isopycnal tilt has the opposite orientation to the continental slope [Wang and Ikeda, 1997a]. At the open boundaries, in situ temperature and salinity vertical profiles, which were obtained by CTD (conductivity, temperature, depth) on the T/S *Oshoro-maru* in 2001, were used in this model. Additionally, a sinusoidal perturbation on the initial geostrophic flow, P_u , was given by equation (1) following Wang and Ikeda [1997b]:

$$P_u = 0.1 \sin\left(\frac{2\pi}{L_x}x\right) \exp\left[-\left(\frac{y-y_0}{a}\right)^2\right] \quad (1)$$

where L_x is the wavelength, y_0 is the location of the front, and a is the width of the front ($1.8 \text{ Rd} = 19 \text{ km}$). In section 4.1, we will decide the best values of L_x and y_0 to reproduce the eddy field. This horizontal sinusoidal perturbation of the initial geostrophic velocity field is given to accelerate the development of unstable waves.

[16] Constant effective horizontal eddy viscosity and diffusivity P_e were calculated using Smagorinsky's [1963]

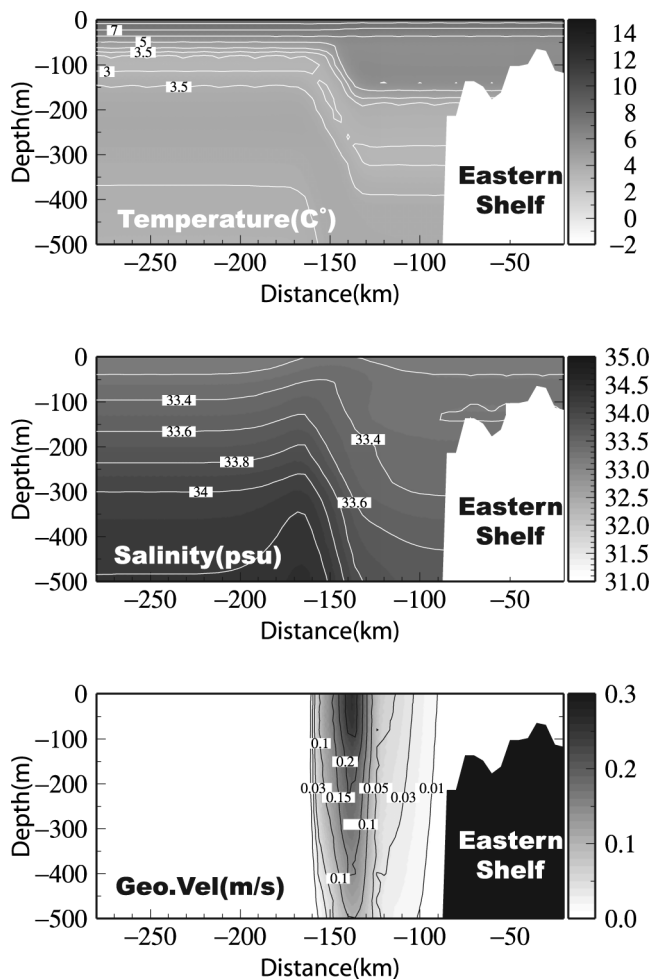


Figure 4. Initial conditions of temperature (upper), salinity (middle), and northwestward geostrophic velocity (lower) for numerical modeling are shown.

formulation, and effective vertical eddy viscosity and diffusivity were calculated by a second-order turbulent closure scheme [Mellor and Yamada, 1982]. Due to using the semi-implicit scheme, the time step is 120 s, which is six times larger than the Courant, Friedrich, and Lewy (CFL) condition [Wang, 1996]. The model was integrated to 40 days.

[17] In this modeling study, we first explored optimal conditions of mesoscale eddy generation by changing the distance between the jet flow and the shelf break, and the wavelength of the baroclinic instability wave. Then we carried out tracer experiments of eddy-related cross-slope exchange with nondimensional tracer under $\sigma = -0.115$ over the basin or above $\sigma = -0.08$ over the shelf. The former tracer was the assumed basin nutrient concentrations and the latter tracer was the high *Chl-a* concentration assumed to exist in shelf waters.

3. Hydrographic Observations

3.1. Anticyclonic Eddies in 2001

[18] A positive SLA field at the Bering Sea shelf break was observed from July 25 to 26, 2001 (Figure 3a). The geostrophic section plot shows a maximum northwestward component of 27.7 cm s^{-1} at 55.78°N and a southeastward

component of 24.2 cm s^{-1} at 55.9°N (Figure 5a). These two components have a magnitude of more than 15 cm s^{-1} at over 400 m depth. A northwestward component of about 21.4 cm s^{-1} was also estimated at about 56°N . This three-band structure of geostrophic current is due to the meander of the BSC or eddies [e.g., Kinder *et al.*, 1975, 1980]. Figure 5a also shows a northwestward component of 20 cm s^{-1} at about 56.3°N and southeastward components of about 15 and 6.5 cm s^{-1} at 56.2°N and 56.47°N , respectively. These indicate that there were small scale cyclonic and anticyclonic eddies centered at 56.27°N and 56.4°N in the shelf. In the basin area, no significant geostrophic component was recognized. Thus our observations revealed that the Bering Sea shelf break is an eddy-rich area. Figure 5b illustrates the section of potential temperature. At less than 50 m depth, a warm layer of more than 7°C formed in the basin area. This warm layer, however, deepened at about 55.84°N and 56.34°N in the shelf, due to mixing by small scale anticyclonic eddies and perhaps by tides. In the basin, cold water less than 3.5°C called the dichothermal water [Miura *et al.*, 2002, 2003], existed at the 100 m to 200 m depth from 55.4°N to 55.6°N . Density structure (Figure 5c) showed isopycnals tilted in the opposite direction, but down-bowed isopycnals existed at 55.84°N . At the shelf break, the 5°C isotherm and 26 kg m^{-3} isopycnal were tilted, indicating the shelf break front (Figures 5b and 5c).

[19] According to Figures 5a–5c, we believe our observation captured an anticyclonic eddy with diameter of about $50 \sim 70 \text{ km}$ centered at 55.84°N . In addition, low nitrate-nitrite concentrations were found at the center of the eddy (Figure 5d). These indicate the anticyclonic eddy drove the isopycnals downward, mixing cold water with surface warm water resulting in low nutrient [Mizobata *et al.*, 2002]. Conversely, isopycnals were bent upward and relatively high nitrate-nitrite concentrations of about 15 to $20 \mu\text{M}$ were observed in the subsurface layer from 56°N to the shelf area at about 56.3°N (Figures 5c and 5d). This high nitrate-nitrite layer could have originated in the basin. At the shelf break, temperature and density were uniform at depths less than 50 m depth, indicating that basin water can be transported to the shelf easily (Figures 5b and 5c). Therefore, high nitrate-nitrite waters were distributed under the shelf break front (Figures 5c and 5d). Phosphorus distribution in 2001 was very similar with nitrate-nitrite distribution showing the low concentration in the surface layer, upwelling at the shelf break, and high concentration in the subsurface layer at the shelf break and shelf (not shown).

[20] High *Chl-a* concentrations ($3 \sim 10 \text{ mg m}^{-3}$) were observed in the surface layer ($0 \sim 50 \text{ m}$ depth) at 56.6 to 55.8°N between an anticyclonic eddy and the shelf break (Figure 5e). Especially high values of *Chl-a* were 12.79 mg m^{-3} at 30 m depth (55.84°N), 19.75 mg m^{-3} at 20 m depth (56.09°N), 11.0 mg m^{-3} at 10 m depth (56.34°N), and 10.32 mg m^{-3} at 10 m depth (56.58°N).

3.2. Anticyclonic Eddies in 2002

[21] A positive SLA field detached from offshore was observed from August 8 to 9, 2002 (Figure 3b). The hydrographic section shows a maximum northwestward geostrophic velocity of 22.1 cm s^{-1} at 55.5°N and a southeastward component of 17.4 cm s^{-1} at 55.62°N (Figure 6a). A broad southeastward component occupied

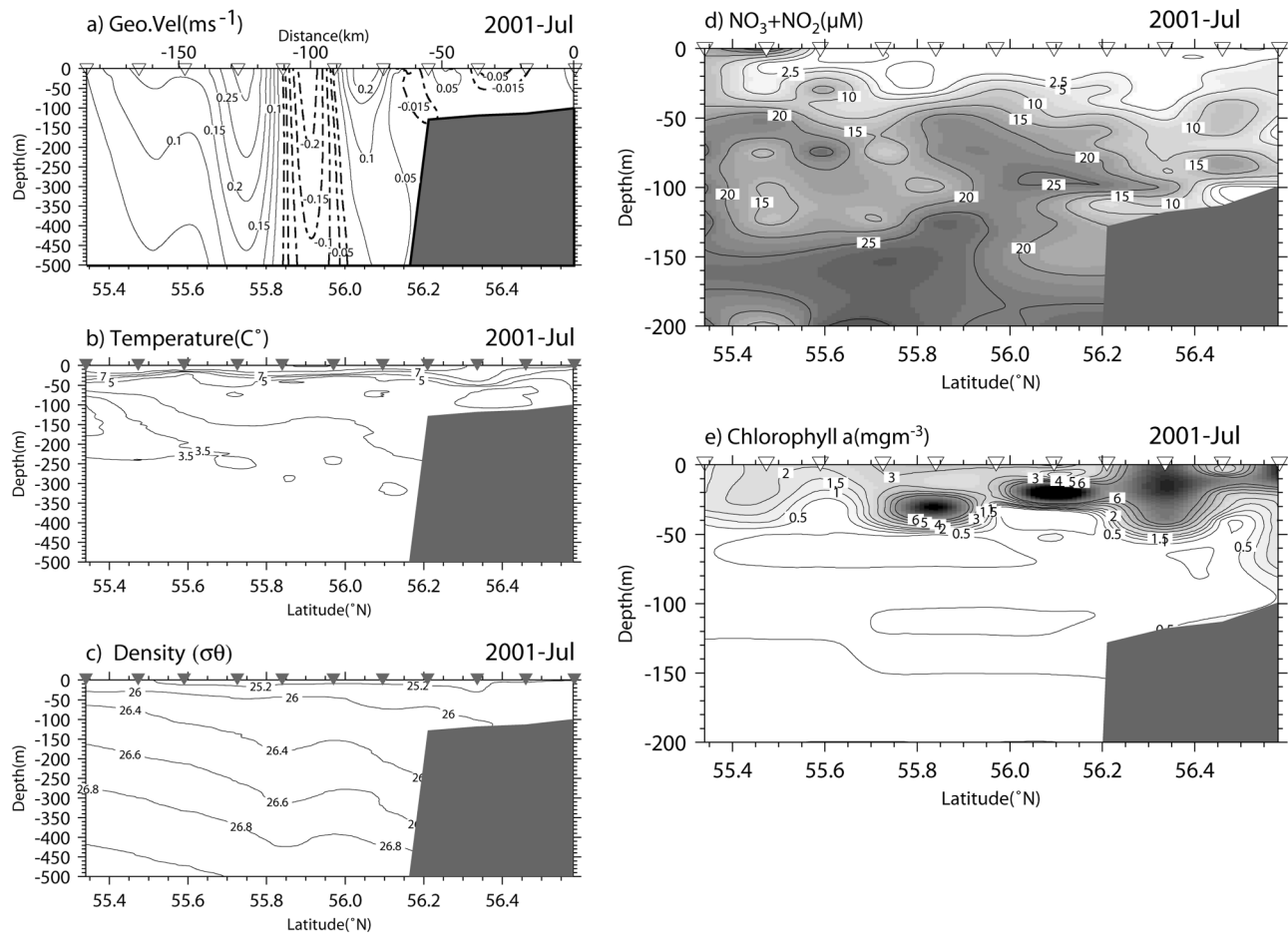


Figure 5. Cross sections of (a) geostrophic velocity, (b) temperature, (c) density, (d) nitrate and nitrite concentration, and (e) chlorophyll-a concentration from hydrographic observations in 2001 are shown. Black and white triangles indicate the oceanographic stations.

from 55.6°N to about 55.85°N, and a weak northwestward component was at the shelf break. The geostrophic structure of this eddy was relatively shallow compared with the eddy observed in 2001 (Figure 6a). Southeastward geostrophic velocity at the 200 m depth is 10 cm s⁻¹ from 55.6°N to 55.65°N. The BSC and its related eddies reach to 500 m depth at least, and usually extend to over 1000 m depth [Mizobata *et al.*, 2002; Johnson *et al.*, 2004]. Figure 7 represents SLA maps from July 31 to September 18 in 2002. The anticyclonic eddy which we observed decayed at 55.5°N, 171.5°W on July 31 (Figure 7a) and then developed again at the end of July (Figure 7b). After developing, the magnitude and size of this eddy were maintained during August (Figure 7c). Finally this eddy decayed and coalesced with another large anticyclonic eddy located at 54.5°N, 173°W (Figure 7d). Thus shallow geostrophic structure and SLA distributions reflect the developing stage of the eddy or the meander. About 50 km offshore from the shelf break a three-band structure of geostrophic velocity was defined, but no distinctive geostrophic component was detected. Therefore, the eddy and the meander of the BSC separated at least 50 km offshore from the shelf break.

[22] A surface warm layer more than 7°C was formed, and bent downward near 55.6°N (Figure 6b). Dichothermal water was also found from 150 m depth to 300 m depth at

55.79°N, similar to what was found in the summer of 2001 (Figure 5b). The section of water density shows that isopycnals bowed downward at 55.59°N and upward at 55.93°N (Figure 6c).

[23] From the result of geostrophic calculation and a SLA map, we captured the southeast edge of an anticyclonic eddy (Figure 3b). As was observed in 2001, cold water was only seen at the edge of the eddy (55.79°N, Figure 6b) and isopycnals were tilted downward, advecting surface heat to the subsurface layer by the downwelling at the center of the eddy (Figure 6c). Nitrate-nitrite contours designated clear downward tilting at the center of the eddy and upward tilting at the edge of the eddy, from the surface to 100 m depth (Figure 6d). Different results described above with high *Chl-a* concentrations (1.0 ~ 3 mg m⁻³) were recognized in the surface from the basin to the shelf break (Figure 6e). Especially high *Chl-a* distributions, 4.42 mg m⁻³ and 4.53 mg m⁻³, were found in the surface layer at 55.66°N and 55.73°N, where the geostrophic structure of the eddy is shallow. High nitrate-nitrite concentrations were found from the surface to the bottom near the shelf break, while the downward isolines of nitrate-nitrite appeared around 55.8°N (Figure 6d). Relatively low nitrate-nitrite concentrations around at 55.8°N would be due to the dichothermal water,

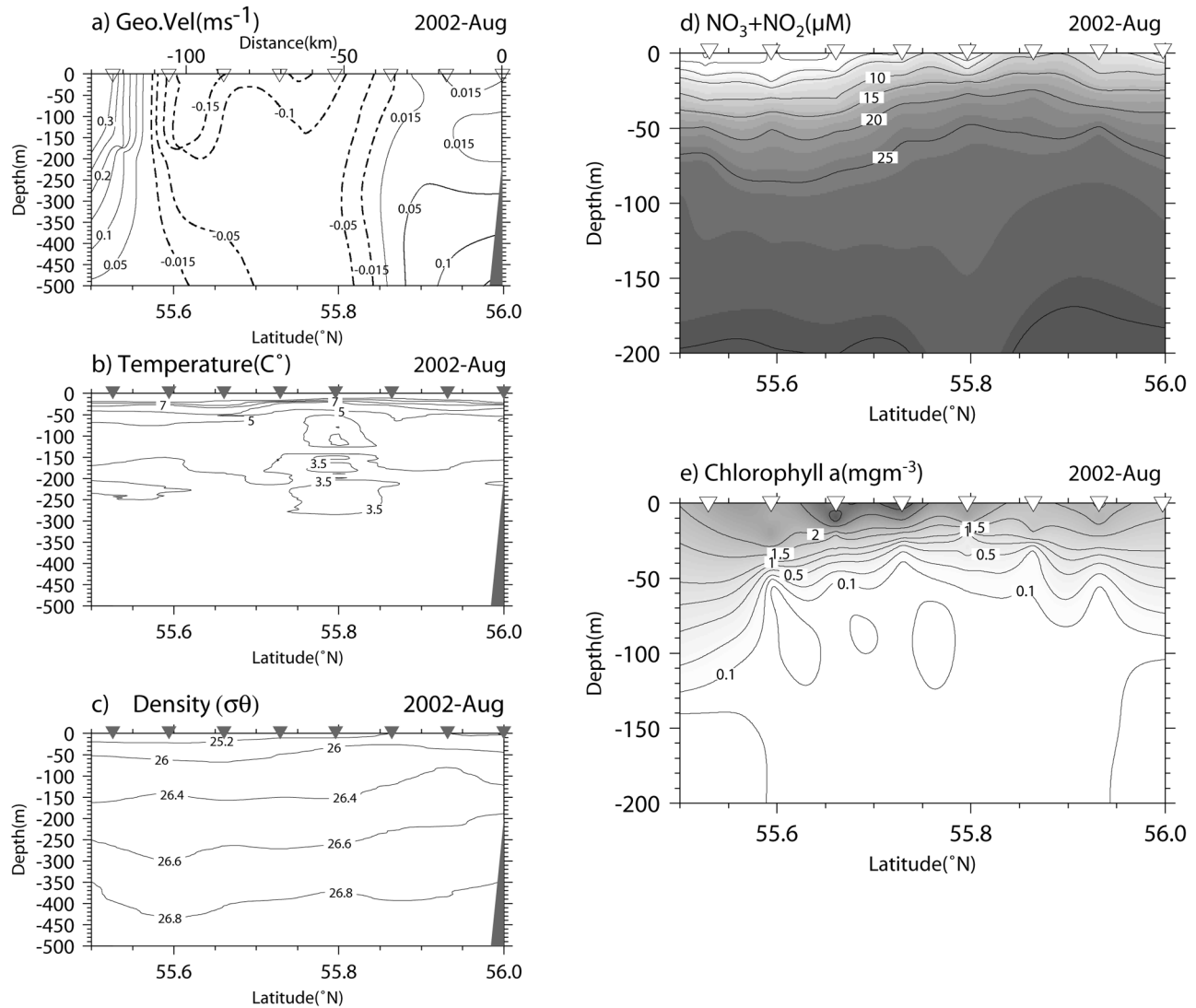


Figure 6. Cross sections of (a) geostrophic velocity, (b) temperature, (c) density, (d) nitrate and nitrite concentration, and (e) chlorophyll-a concentration from hydrographic observations in 2002 are shown. Black and white triangles indicate the oceanographic stations.

because isopycnals do not indicate any downwelling at 55.8°N .

4. Simulations of Eddy-Related Cross-Slope Exchange

4.1. Simulations of the Eddy Field

[24] Optimum conditions for the regeneration of the eddy field were determined from 44 eddy simulations with different locations of jet flow y_0 (0 km, 25 km, 50 km and 75 km offshore from the shelf break) and different wavelengths L_x of barotropic instability (50 km, 55.5 km, 62.5 km, 71 km, 83 km, 100 km, 125 km, 166.6 km, 200 km, 250 km, 500 km) using equation (1). Each wavelength corresponds to a wave number of 10, 9, 8, 7, 6, 5, 4, 3, 2.5, 2, and 1. The evolution of volume averaged eddy kinetic energy (EKE) is shown in Figure 8. Jet flow located above the shelf break results in low EKE, indicating few or small eddies, even though jet flow may have any wave number (Figure 8a). The high averaged EKE value,

when the eddy field is reproduced, is similar to the result in section 3.1, showing a large anticyclonic eddy penetrating to a depth of 500 m. Relatively rapid and high EKE development was preceded by jet flow located 25 km offshore from the shelf break which had wave number of less than 4 (Figure 8b). Jet flow with a wave number of more than 6, however, resulted in lower EKE than seen in Figure 8a. The eddy field is highly developed because jet flow with a barotropic wavelength of 166.6 to 250 km (wave number = 2 ~ 3) was specified at 50 km offshore from the shelf break (Figure 8c). No difference in eddy development was detected when the jet flow was located more than 50 km offshore from the shelf break.

[25] In this study we define the barotropic 200 km-wavelength and a distance between shelf break and jet flow axis of 50 km to be the optimum conditions for the regeneration of the eddy field. Under these conditions, simulations of the eddy field were conducted (Figure 9). Large meandering occurred along the shelf break ($X = 250 \text{ km} \sim 350$, $Y = 100 \text{ km} \sim 200 \text{ km}$) on day 20 and resulted

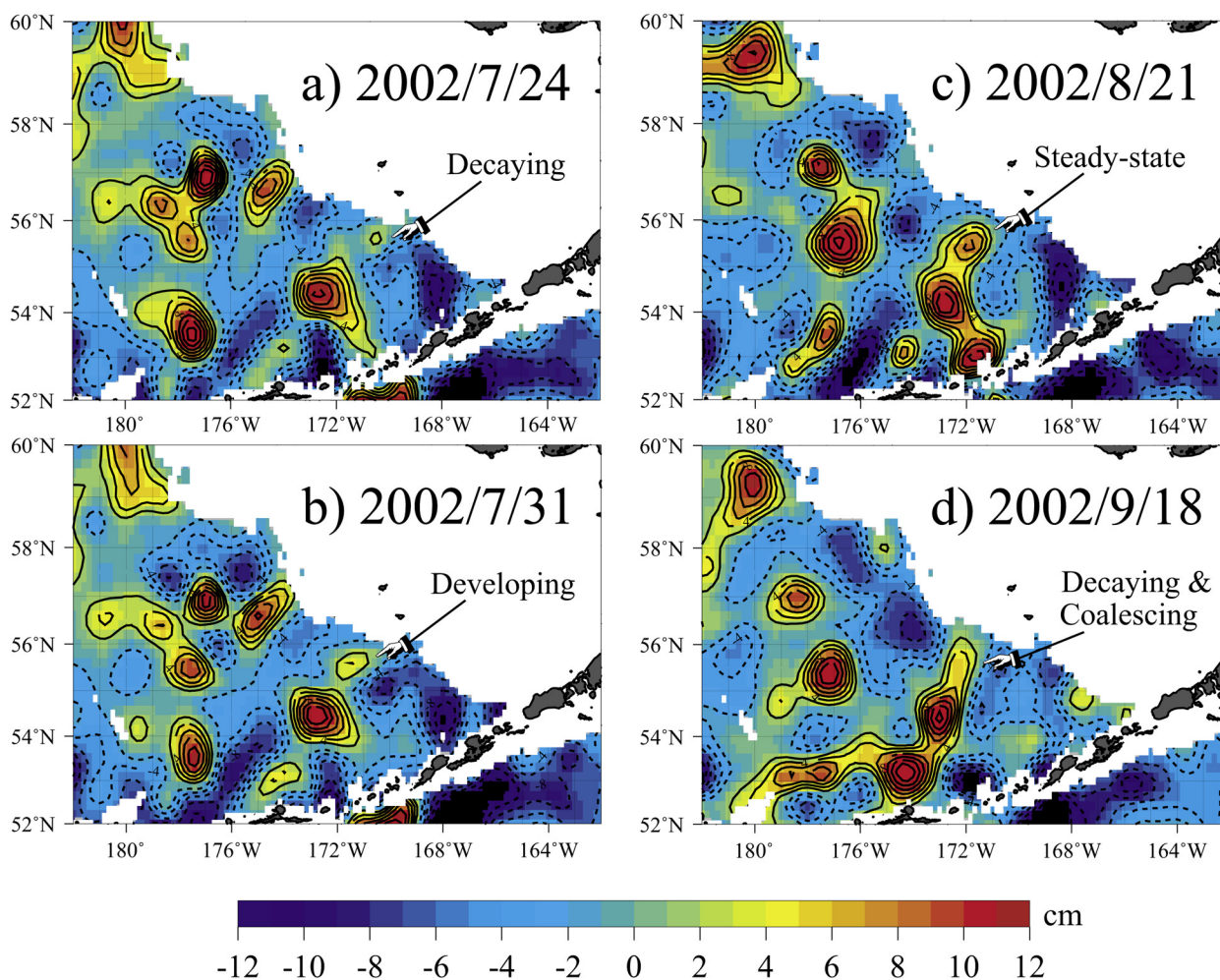


Figure 7. Sea level anomaly (SLA) maps on July 31, August 14, September 4, and September 18 in 2002 are shown.

in the mesoscale anticyclonic eddy on day 30, when small ellipsoidal cyclonic eddies occurred at the northwest and southeast side of this anticyclonic eddy, and other large meanders representing positive sea elevation appeared along the shelf break ($X = 100 \sim 200$ km, $Y = 100 \sim 200$ km; $X = 400 \sim 500$ km, $Y = 150 \sim 250$ km) (Figure 9b). The anticyclonic eddy generated on day 20 propagated northwestward along the shelf break, coalescing in the meander ($X = 100 \sim 300$ km, $Y = 100 \sim 200$ km) on day 40 (Figure 9c). Another meander developed into an anticyclonic eddy and detached offshore ($X = 375 \sim 475$ km, $Y = 100 \sim 150$ km). Cyclonic eddies described above remained between the shelf break and anticyclonic eddies ($X = 200 \sim 250$ km, $Y = 200 \sim 250$ km; $X = 325 \sim 425$ km, $Y = 150 \sim 200$ km).

4.2. Eddy-Induced on-Shelf Nutrient Flux

[26] First we carried out a tracer experiment of basin nutrient. Results of hydrographic surveys show that major nutrients are depleted in the surface layer, but are abundant at the subsurface layer in the basin during summer (Figure 5a). An upwelling-like event related to the mesoscale eddy is also indicated in Figure 5. Therefore, we need

to consider how basin nutrients in the subsurface layer are transported to the shelf break by mesoscale eddies. A passive tracer, assumed basin nutrients, was introduced into the basin from the fourth layer to the bottom in the basin at time 0. A tracer concentration of 20 reflects the average nitrate-nitrite concentration. Integrated on-shelf flux under $\sigma = -0.115$ at 200 m depth is superimposed on Figure 9.

[27] On day 20 when EKE development was initiated, integrated on-shelf fluxes occurred at the shelf near $X = 250$ km and $X = 350 \sim 400$ km at the location of a large meander's edge (Figure 9a). Integrated on-shelf fluxes increased when the anticyclonic eddy was regenerated on day 30 (Figure 9b). Relatively large on-shelf flux emerged near the cyclonic eddies on the side of the anticyclonic eddy. Other increases in integrated on-shelf fluxes were exhibited near the meander at $X = 375 \sim 450$ km. The area where on-shelf fluxes were initiated shifted northwestward following the occurrence of an anticyclonic eddy (Figure 9c). A considerable increase in on-shelf fluxes was recognized at the shelf near $X = 250$ km where the cyclonic eddy remained. On-shelf fluxes ($X = 350$ km) also occurred near another cyclonic eddy, while on-shelf fluxes almost disap-

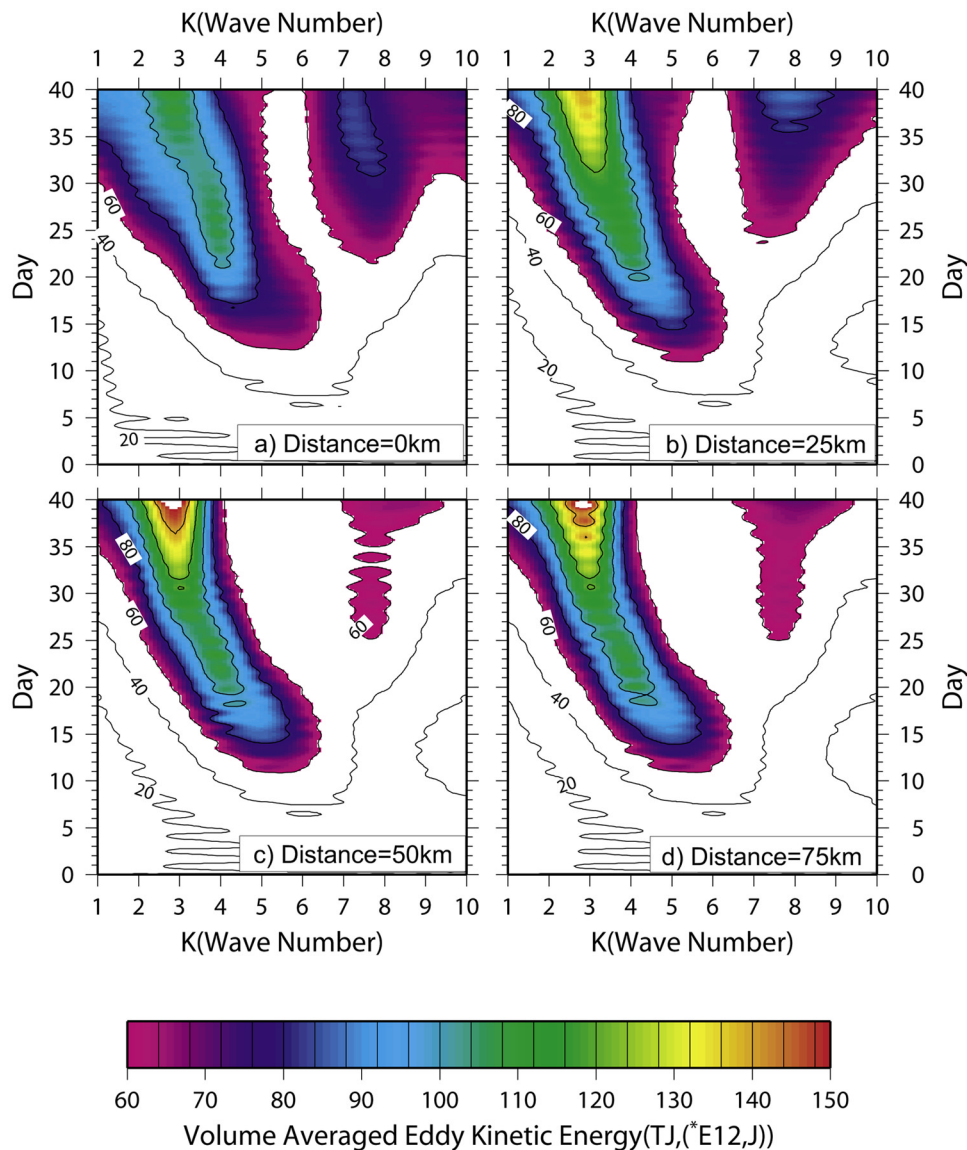


Figure 8. Evolution of volume averaged eddy kinetic energy when the distance between the self break and jet flow is (a) 0 km, (b) 25 km, (c) 50 km, and (d) 75 km is shown.

peared at the shelf near $X = 400 \sim 500$ km, where the anticyclonic eddy detached offshore.

[28] Figure 10 shows the time series of the amount of on-shelf nitrate-nitrite fluxes when the eddy field was either regenerated or not. Numerical simulation without perturbation given equation (1) resulted in no eddy and low on-shelf fluxes (dashed line of Figure 10). The maximum amount of on-shelf flux was about 1.0×10^3 ($\text{m}^3 \text{s}^{-1} \times \mu\text{M}$). However, a numerical simulation with perturbation showed a larger amount of on-shelf flux after day 10, and the maximum amount of on-shelf flux was close to 2.0×10^3 ($\text{m}^3 \text{s}^{-1} \times \mu\text{M}$). Eventually, regeneration and propagation of eddies results in about a 64.53% increase in the on-shelf fluxes.

[29] Tracer in the basin, which was assumed nutrients, should be transported to the shelf by the upwelling/advection/diffusion. To explore the mechanisms of shelf-ward transport, the comparisons between the vertical velocity field and the vertical diffusivity field at 180 m depth are

shown in Figure 11. To compare the magnitudes of the vertical velocity and vertical diffusivity, Figures 11d–11f represent the values which are derived from $(\text{vertical diffusivity})/(\text{vertical grid size (40 m)})$.

[30] Figure 11a demonstrates that a vertical velocity field was developed on day 20. Upwelling and downwelling occurred to the southeast and northwest sides of the meander ($X = 250 \sim 300$ km; $X = 350 \sim 400$ km). This result is same as that of Wang and Ikeda [1997b]. Upward and downward velocity related to the meander of jet flow and anticyclonic eddy were also observed. These vertical velocities should enhance nutrient concentration at the surface layer, transporting nutrient-rich water from the bottom, and surface waters with low nutrients to the bottom. On day 30, the magnitude of vertical velocity was decreased (Figure 11b). On-shelf fluxes were estimated near the cyclonic eddy and the anticyclonic eddy, while weak downwelling and upwelling occurred at the shelf break ($X = 200 \sim 250$ km, $Y = 225$ km; $X = 300 \sim 350$ km, $Y =$

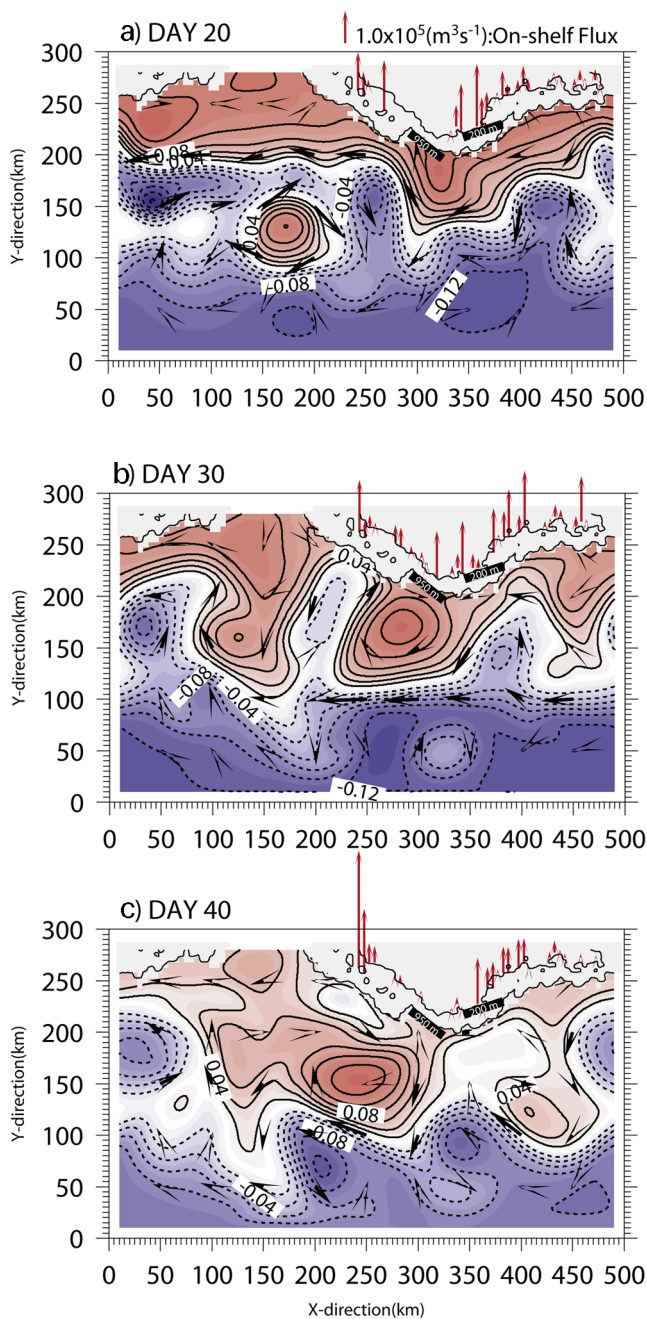


Figure 9. Surface elevation and on-shelf fluxes on day (a) 20, (b) 30, and (c) 40 are shown. Red and blue colors mean positive and negative surface elevations, respectively. Red arrows indicate on-shelf fluxes.

200 km). Although a downwelling exists at the shelf break ($X = 200 \sim 250$ km, $Y = 225$ km), there was an increase in on-shelf flux at the shelf (Figure 11c).

[31] The magnitude of vertical diffusivity was much smaller than that of vertical velocity by an order of $10^3 \text{ cm}^2 \text{ s}^{-1}$ (Figures 11d–11f). Relatively high vertical diffusivities were found at the axis of jet flow and around the anticyclonic eddy. The vertical diffusivity field was most developed on day 30 (Figure 11e), when the anticyclonic eddy was formed at the shelf break. On day 40, the magnitude of vertical diffusivity dropped immediately

(Figure 11f), even around the anticyclonic eddy ($X = 200 \sim 300$ km, $Y = 100 \sim 200$ km).

[32] Figure 11 indicates that nutrients are transported to the surface layer by vertical velocity advection before the eddy is formed. Vertical diffusivity is developed when the eddy is formed. Thus the eddy generation inducing vertical mixing and diffusion is crucially important for supplying nutrients from the subsurface layer to the surface layer. Additionally, horizontal advection is important for shelf-ward transport of nutrients according to Figures 10 and 11, because compared to the advection timescale, the magnitude of the vertical diffusivity timescale is secondary.

4.3. Basin-Ward Transport of High Chl-a Waters

[33] Under conditions the same as those described above, a tracer experiment was carried out to measure the surface water exchange. We released the tracer assumed to contain a high *Chl-a* concentration into the first layer to the third layer in the shelf at time 0. A tracer concentration of 5 is considered the high *Chl-a* concentration in the shelf and shelf break region. The results indicate that surface waters in the shelf were advected to about 100 km basin-ward from the shelf break by the regeneration and propagation of the eddy field (Figure 12). On day 20, surface waters were advected from the shelf break to the basin following the development of the eddy field (Figure 12a). In particular, basin-ward transports were found at the shelf break, $X = 225 \sim 250$ km and $X = 350$ km, where offshore components are thought to be large because of the jet flow and the meander. On day 30, the meander and the anticyclonic eddy drew surface waters, while low concentrations of surface tracer were found around the cyclonic eddy (Figure 12b). On day 40, the tracer was widely distributed from the shelf break to the basin (Figure 12c). The tracer was transported by the advection of the anticyclonic eddy ($X = 100 \sim 350$ km, $Y = 25 \sim 250$ km) and by the eddy's basin-ward propagation ($X = 400 \sim 500$ km, $Y = 100 \sim 200$ km). Thus the area where the tracer was distributed depended on the scale of eddies and the length of eddy passage along the shelf break. The on-shelf fluxes in the surface layer ($\sigma = 0.0 \sim -0.08$) detected by the drifting buoy studies (Figure 2), however, could not be simulated in this study. This implies that on-shelf flux in the surface layer is a rare event, but on-shelf flux induced by eddies in the subsurface layer is more common.

5. Conclusions and Discussion

5.1. Cause of Eddy Field Development

[34] Results from in situ observations in 2001 show that the gradient of isopycnals tilts in a direction opposite to that of the topographic slope, in which the unstable wave numbers moves to a high wave number (short wave). The same situations have been observed and have induced short unstable waves [Wang and Ikeda, 1997b, 1997c].

[35] Sensitivity analysis of eddy development indicates that the highest eddy activity can be reproduced when jet flow with a 200 km-wavelength is introduced at a distance greater than 50 km basin-ward from the shelf break. Jet flow near the shelf break does not introduce baroclinic waves because the magnitude of shear on the coastal side is greater than that on the offshore side [Shimada and Kubokawa,

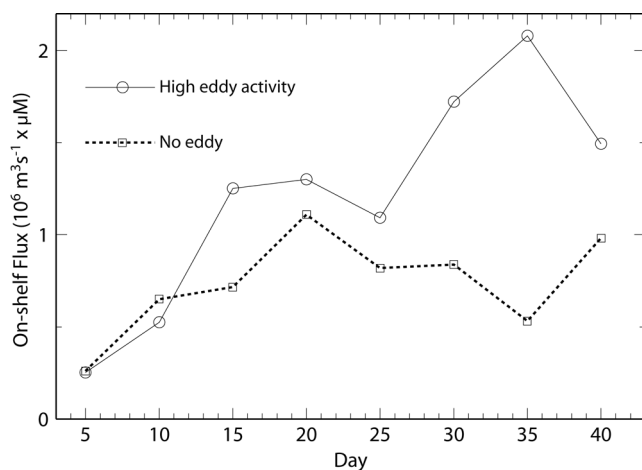


Figure 10. Time series of integrated on-shelf nitrate + nitrite fluxes derived from numerical modeling is shown. Black and dotted line represent on-shelf fluxes when (a) eddy or (b) no eddy is generated at the shelf break.

1997], and bottom and lateral dissipation are large in this case. The 50 km distance from the shelf break is plausible because the axis of the BSC has a lateral scale of about 100 km [Johnson *et al.*, 2004].

[36] The baroclinic instability of the jet flow is also important for eddy development. This instability is most likely introduced by the Aleutian North Slope Current (ANSC) which is the main origin of the BSC [Schumacher and Stabeno, 1994; Reed and Stabeno, 1999]. Transport of the ANSC is affected by the inflow from Aleutian passes [Reed and Stabeno, 1994] and is accelerated after the ANSC turns to the northwestward near the Umnak Plateau [Stabeno and van Meurs, 1999]. Furthermore the instability near Amchitka Pass results from an increase in inflow influenced by the Alaskan Stream eddy [Okkonen, 1996]. There is another possibility; that baroclinic instability is related to the dynamics between relatively fresh water in the shelf and saline water in the basin. In the Gulf of Alaska, Lorenzo *et al.* [2005] demonstrated that the generation mechanism of the Haida eddies is associated with the mean advection of warmer and fresher water masses. The effect of relatively fresh shelf water on the eddy field will be investigated in the future.

[37] Along the Bering Sea shelf break, the eddy field is developed beginning in spring and high eddy activity can be seen during summer [Mizobata and Saitoh, 2004]. The results described above indicate that the condition provoking the eddy field is introduced along the Bering Sea shelf break during summer.

5.2. Mechanisms Maintaining the High Primary Productivity in the Bering Sea Green Belt

[38] Simulation results revealed that basin nutrient-rich water under $\sigma = -0.115$ was transported to the shelf when the eddy field was regenerated (Figure 9), while a relatively high concentration (15 ~ 20 μM) of basin nutrients was distributed between the periphery of an anticyclonic eddy and the shelf break in the summer of 2001 (Figure 5d). Simulation results also imply that an increase in on-shelf fluxes due to the eddy field should always occur (Figure 10).

Thus, on-shelf flux by eddy in the subsurface layer is more important for nutrient supply than surface cross-slope flows. Vertical velocity and horizontal advection/diffusion related to the eddy field will transport basin nutrients into the shelf region at 200 m isobaths, at least (Figures 10 and 11). Eddy-induced nutrients will be transported to the stabilized water column at the shelf break front (Figures 5b and 5c) maintaining the phytoplankton in the euphotic zone [Springer *et al.*, 1996], and resulting in high phytoplankton biomass at the shelf break. We believe high *Chl-a* waters with low nutrient concentration in the surface layer of the shelf break reflect these phenomena (Figure 5). In this study, we used only nitrate-nitrite data to show nutrient depletion at the shelf break. Other measured nutrients (phosphate and silicate) were also depleted in the surface layer at the shelf break (not shown). Only Nitrate-nitrite data alone is sufficient to explain nutrient limitation in this area, but further research will be needed to study the uptake and export of other major nutrients. Nutrients transported by cross-slope exchange will be trapped by tidal current around the Pribilof Islands [Kowalik and Stabeno, 1999] and affect lower trophic levels.

[39] Conversely, surface waters in the shelf were transported to the basin by eddy regeneration and propagation, and extended along the shelf break 100 km offshore from the shelf break (Figure 12). Moreover, the area where surface *Chl-a* waters were distributed was expanded to include the basin that is the HNLC region, by northwestward and basin-ward movement of the eddy (Figure 12). In situ observations in the summer of 2001 and 2002 revealed the high *Chl-a* waters between the anticyclonic eddy and the shelf break (Figures 5e and 6e).

[40] To explain the Bering Sea Green Belt, “the iron curtain hypothesis”, which attributes high primary production to nitrate from the basin and iron from the shelf, has been considered (P. McRoy, personal communication). Over the continental shelf, iron concentration is usually higher than in open water [Sunda, 2001]. However, no iron data exist for in the Bering Sea shelf. If there is high iron concentration in the shelf, mesoscale eddies along the shelf break can carry iron-rich shelf water into the HNLC basin area. Recent work on iron transport by the Haida eddies in the Gulf of Alaska [Johnson *et al.*, 2005] demonstrated that upward transport along isopycnals and upwelling due to eddy decay provide iron flux into the euphotic zone. In the Bering Sea basin area, Takata *et al.* [2005] measured high concentration of dissolved iron and dissolvable iron (0.4 ~ 1.5 nM and 2.3 nM, respectively) in the intermediate water (200–1500 m water depth). Bering Sea mesoscale eddies usually penetrate more than 1000 m water depth [Johnson *et al.*, 2004]. Therefore Bering Sea eddies in the basin can supply iron from the intermediate water to the euphotic zone when eddies decay [Bakun, 1996]. Thus Bering Sea eddies would supply macronutrients (e.g., nitrogen) in the basin and iron in the shelf and deep basin to the shelf break area, resulting in better conditions for the phytoplankton. This hypothesis is supported by the hydrographic survey in 2001 (Figure 5) showing high *Chl-a* values at the shelf break.

[41] In summary, eddy generation and propagation along the shelf break contributes to (1) an increase in on-shelf nutrient fluxes maintaining high primary productivity in the subsurface layer from the basin, and (2) the basin-ward

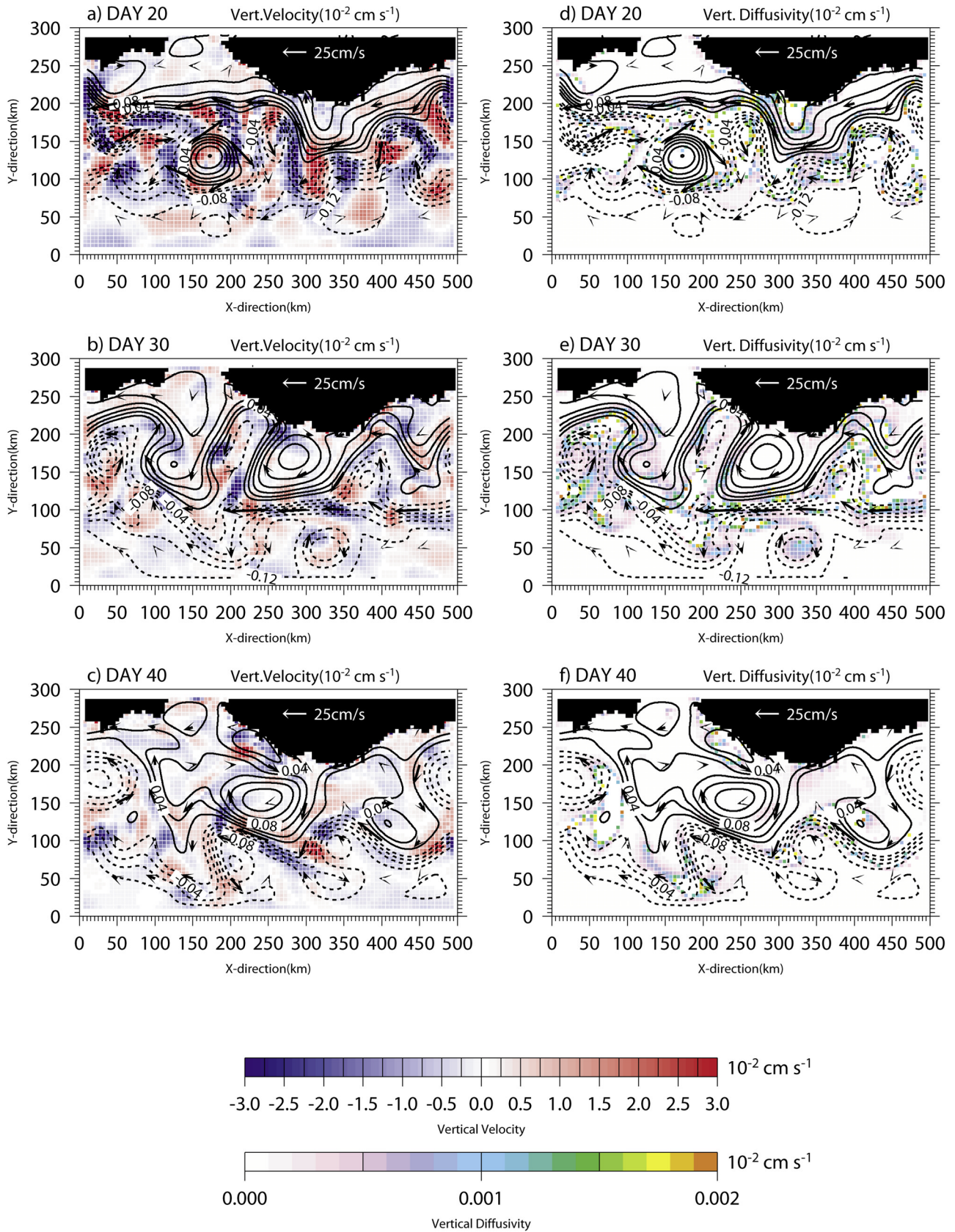


Figure 11. Surface elevations, geostrophic velocities with 180-m vertical velocities (a, b, and c) and vertical diffusivities (d, e, and f) on day 20, 30, and 40 are shown.

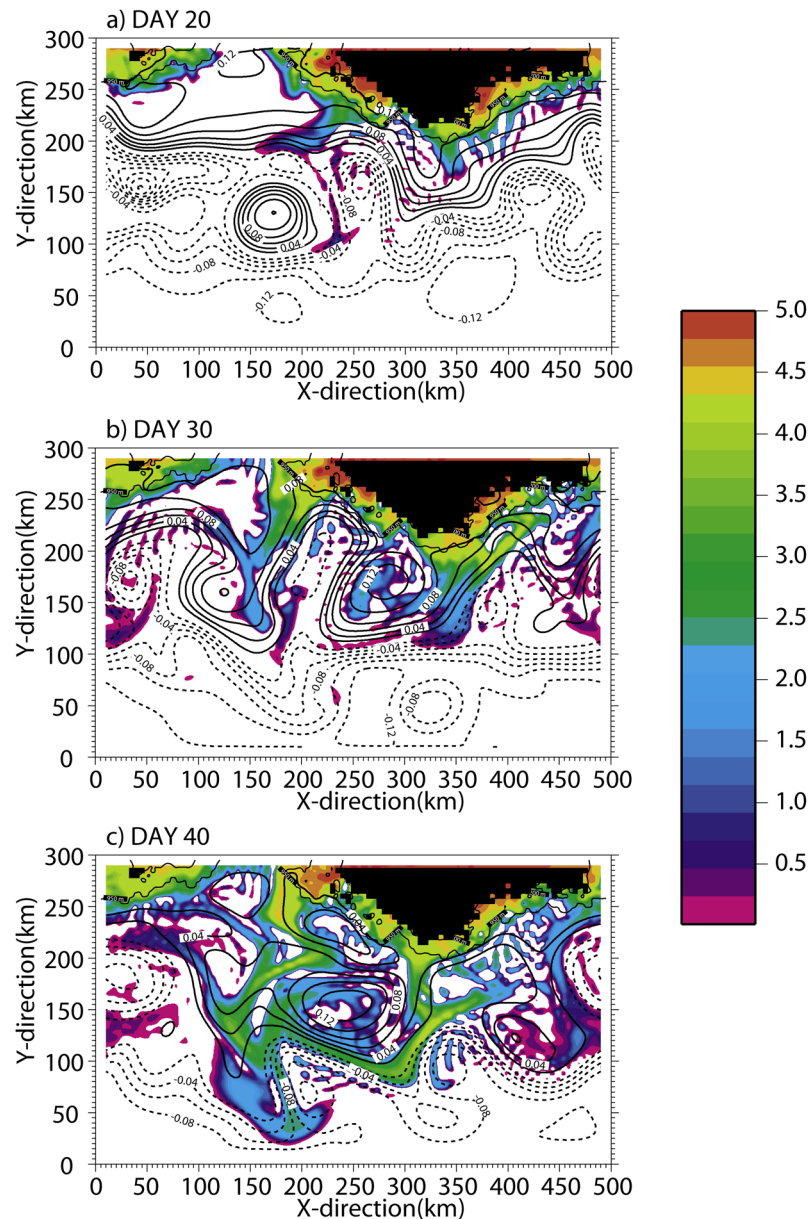


Figure 12. Basin-ward transport of surface tracer assuming high chl-*a* waters at the shelf break at day (a) 20, (b) 30, and (c) 40.

transport of surface high *Chl-a* waters resulting in an expanding Bering Sea Green Belt.

[42] In this study, we explained the cross-slope exchange and its effects on primary productivity and on-shelf fluxes detected by drifting buoy. Our results support the hypothesis that inter-annual variability of primary production of the Bering Sea Green Belt primary productivity is associated with the fluctuation of the eddy field, as reported by Mizobata and Saitoh [2004]. Eddy-induced on-shelf nutrients flux should affect the marine ecosystem at the highly productive fishing ground located at the shelf break and on the shelf. In the future, a finer resolution ocean model will be applied to estimate precise on-shelf transport by eddies.

[43] **Acknowledgments.** We thank Motoyoshi Ikeda for his valued and constructive comments. We are deeply grateful for the constructive

comments of the anonymous reviewers. We also thank the captain and crew of the T/S *Oshoro-maru*. A part of this study is supported by the Japan Aerospace Exploration Agency (JAXA) through the program of Arctic Research projects using the IARC (International Arctic Research Center)-JAXA Information System (IJIS). We appreciate all the help and support of the research institutes concerned, including the International Arctic Research Center, University of Alaska Fairbanks, and Japan Agency for Marine-Earth Science and Technology (JAMSTEC). All figures were described using the Generic Mapping Tool (GMT).

References

- Arakawa, A., and V. R. Lamb (1977), Computational design of the basic dynamic processes of the UCLA General Circulation Model, in general circulation models of the atmosphere, in *Methods in Computational Physics: Advances in Research and Applications*, edited by J. Chang, pp. 173–265, Elsevier, New York.
- Bakun, A. (1996), Patterns in the ocean: Ocean processes and marine population dynamics, pp. 1–323, Calif. Sea Grant Coll. Syst., La Jolla.
- Bering Sea Ecosystem Study (BEST) (2003), Bering Sea Ecosystem Study (BEST) draft science plan. (Available at http://www.arcus.org/bering/science_plan.html)

- Blumberg, A. F. (1991), A primer for ECOM-si, technical report, p. 66, HydroQual, Inc., Mahwah, N. J.
- Blumberg, A. F., and G. L. Mellor (1987), A description of a three-dimensional coastal ocean circulation model, in *Three-Dimensional Coastal Ocean Models*, vol. 4, edited by N. Heaps, 208 pp., AGU, Washington, D. C.
- Casulli, V. (1990), Semi-implicit finite-difference methods for the two-dimensional shallow water equations, *J. Comput. Phys.*, *86*, 56–74.
- Johnson, G. C., P. J. Stabeno, and S. C. Riser (2004), The Bering Slope Current System revisited, *J. Phys. Oceanogr.*, *34*, 384–398.
- Johnson, W. K., L. A. Miller, N. E. Sutherland, and C. S. Wong (2005), Iron transport by mesoscale Haida eddies in the Gulf of Alaska, *Deep Sea Res., Part II*, *52*, 933–953.
- Kinder, T. H., L. K. Coachman, and J. A. Galt (1975), The Bering Slope Current system, *J. Phys. Oceanogr.*, *5*, 231–244.
- Kinder, T. H., J. D. Schumacher, and D. V. Hansen (1980), Observation of a baroclinic eddy: an example of mesoscale variability in the Bering Sea, *J. Phys. Oceanogr.*, *10*, 1228–1245.
- Kowalik, Z., and P. Stabeno (1999), Trapped motion around the Pribilof Islands in the Bering Sea, *J. Geophys. Res.*, *104*, 25,667–25,684.
- Ladd, C., P. J. Stabeno, and E. D. Cokelet (2005), A note on cross-shelf exchange in the northern Gulf of Alaska, *Deep Sea Res., Part II*, *52*, 667–679.
- Lin, G., and J. F. Atkinson (2000), A mechanism for offshore transport across the Gulf Stream, *J. Phys. Oceanogr.*, *30*, 225–232.
- Lorenzo, E. D., M. G. G. Foreman, and W. R. Crawford (2005), Modeling the generation of Haida eddies, *Deep Sea Res., Part II*, *52*, 853–873.
- Mackas, D. L., and M. D. Galbraith (2002), Zooplankton distribution and dynamics in a North Pacific eddy of coastal origin: I. Transport and loss of continental margin species, *J. Oceanogr.*, *58*, 725–738.
- Mellor, G. L., and T. Yamada (1982), Development of a turbulence closure model for geophysical fluid problems, *Rev. Geophys.*, *20*(4), 851–875.
- Miller, A. J., et al. (1999), Observing and modeling the California Current System, *Eos Trans. AGU*, *80*, 533–539.
- Miura, T., T. Suga, and K. Hanawa (2002), Winter mixed layer and formation of dichothermal water in the Bering Sea, *J. Oceanogr.*, *58*, 815–823.
- Miura, T., T. Suga, and K. Hanawa (2003), Numerical study of formation of dichothermal water in the Bering Sea, *J. Oceanogr.*, *59*, 369–376.
- Mizobata, K., and S. Saitoh (2003), Characteristics of cyclonic and anti-cyclonic eddies in the southeastern Bering Sea 1998–2000 using TOPEX/Poseidon, *Proc. SPIE*, *4892*, 473–481.
- Mizobata, K., and S. Saitoh (2004), Variability of Bering Sea eddies and primary productivity along the shelf edge during 1998–2000 using satellite multi-sensor remote sensing, *J. Mar. Syst.*, *50*, 101–111.
- Mizobata, K., S. Saitoh, S. Shiimoto, T. Miyamura, N. Shiga, M. Toratani, Y. Kajiwara, and K. Sasaoka (2002), Bering Sea cyclonic and anti-cyclonic eddies observed during summer 2000 and 2001, *Prog. Oceanogr.*, *55*, 65–75.
- Okkonen, S. R. (1996), The influence of an Alaskan Stream eddy on flow through Amchitka Pass, *J. Geophys. Res.*, *101*, 8839–8851.
- Okkonen, S. R. (2001), Altimeter observations of the Bering Slope Current eddy field, *J. Geophys. Res.*, *106*, 2465–2476.
- Okkonen, S. R., G. M. Schmidt, E. D. Cokelet, and P. J. Stabeno (2004), Satellite and hydrographic observations of the Bering Sea ‘Green Belt’, *Deep Sea Res., Part II*, *51*, 1033–1051.
- Peterson, T. D., F. A. Whitney, and P. J. Harrison (2005), Macronutrient dynamics in an anti-cyclonic mesoscale eddy in the Gulf of Alaska, *Deep Sea Res., Part II*, *52*, 909–932.
- Reed, R. K., and P. J. Stabeno (1994), Flow along and across the Aleutian Ridge, *J. Mar. Res.*, *52*, 639–648.
- Reed, R. K., and P. J. Stabeno (1999), The Aleutian North Slope Current, in *Dynamics of the Bering Sea*, edited by T. R. Loughlin and K. Ohtani, pp. 177–191, Univ. of Alaska Sea Grant Press, Fairbanks.
- Sapozhnikov, V. V. (1993), Influence of mesoscale anti-cyclonic eddies on the formation of hydrochemical structures in the Bering Sea, *Oceanology*, Engl. Transl., *33*, 299–304.
- Schumacher, J. D., and P. J. Stabeno (1994), Ubiquitous eddies of the eastern Bering Sea and their coincidence with concentrations of larval pollock, *Fish. Oceanogr.*, *3*, 182–190.
- Shimada, K., and A. Kubokawa (1997), Nonlinear evolution of linearly unstable barotropic boundary currents, *J. Phys. Oceanogr.*, *27*, 1326–1348.
- Smagorinsky, J. (1963), General circulation experiments with the primitive equations, I. The basic experiment, *Mon. Weather Rev.*, *91*, 99–164.
- Springer, A. M., C. P. McRoy, and M. V. Flint (1996), The Bering Sea ‘Green Belt’: Shelf edge processes and ecosystem production, *Fish. Oceanogr.*, *5*, 205–223.
- Stabeno, P. J., and P. van Meurs (1999), Evidence of episodic on-shelf flow in the southeastern Bering Sea, *J. Geophys. Res.*, *104*, 29,715–29,720.
- Stabeno, P. J., J. D. Schumacher, and K. Ohtani (1999), The physical oceanography of the Bering Sea, in *Dynamics of the Bering Sea*, edited by T. R. Loughlin and K. Ohtani, pp. 1–28, Univ. of Alaska Sea Grant Press, Fairbanks.
- Sunda, G. S. (2001), Bioavailability and bioaccumulation of iron in the sea, in *The Biogeochemistry of Iron in Seawater*, edited by D. R. Turner and K. A. Hunter, pp. 41–84, John Wiley, Hoboken, N. J.
- Takata, H., K. Kuma, Y. Isoda, H. Kuroda, and T. Senju (2005), Comparative vertical distributions of iron in the Japan Sea, the Bering Sea, and the western North Pacific Ocean, *J. Geophys. Res.*, *110*, C07004, doi:10.1029/2004JC002783.
- Wang, J. (1996), On global stability of the 2-D shallow water equations: an application of the root’s distributive theorem for polynomials in the unit circle, *Mon. Weather Rev.*, *124*, 1301–1310.
- Wang, J., and M. Ikeda (1995), Stability analysis of finite difference schemes for inertial oscillations in ocean general circulation models, in *Computer Modeling of Seas and Coastal Regions*, edited by C. A. Brebbia et al., pp. 19–27, Comput. Mech., Billerica, Mass.
- Wang, J., and M. Ikeda (1997a), A 3D ocean general circulation model for mesoscale eddies-II: diagnostic analysis, *Acta Oceanol. Sin.*, *16*, 29–43.
- Wang, J., and M. Ikeda (1997b), Diagnosing ocean unstable baroclinic waves and meanders using the quasigeostrophic equations and Q-vector method, *J. Phys. Oceanogr.*, *27*, 1158–1172.
- Wang, J., and M. Ikeda (1997c), Inertial stability and phase error of time integration schemes in ocean general circulation models, *Mon. Weather Rev.*, *125*, 2316–2327.
- Whitney, F. A., W. R. Crawford, and P. J. Harrison (2005), Physical processes that enhance nutrient transport and primary productivity in the coastal and open ocean of the subarctic NE Pacific, *Deep Sea Res., Part II*, *52*, 681–706.

K. Mizobata and J. Wang, International Arctic Research Center, University of Alaska Fairbanks, 930 Koyukuk Dr., Fairbanks, AK 99775-7335, USA. (kmizobata@iarc.uaf.edu; jwang@iarc.uaf.edu)

S.-I. Saitoh, Laboratory of Marine Bioresource and Environment Sensing, Graduate School of Fisheries Sciences, Hokkaido University, 3-1-1 Minato-cho Hakodate, Hokkaido 041-8611, Japan. (ssaitoh@salmon.fish.hokudai.ac.jp)